

## Article

# Random Numbers Generated Based on Dual-Channel Chaotic Light

Guopeng Liu <sup>1</sup>, Penghua Mu <sup>1,\*</sup>, Kun Wang <sup>1</sup>, Gang Guo <sup>2</sup>, Xintian Liu <sup>2</sup> and Pengfei He <sup>1,\*</sup>

<sup>1</sup> School of Physics and Electronic Information, Yantai University, Yantai 264005, China; liuguopeng1122@163.com (G.L.); wangkun2021@s.ytu.edu.cn (K.W.)

<sup>2</sup> FISEC Infomation Technology Company Limited, Weihai 264200, China; gg87@fisherman-it.com (G.G.); liuxintian@fisherman-it.com (X.L.)

\* Correspondence: ph\_mu@ytu.edu.cn (P.M.); bupt\_hpf@126.com (P.H.)

**Abstract:** This paper presents a chaotic system based on novel semiconductor nanolasers (NLs), systematically analyzing its chaotic region and investigating the influence of key parameters on the unpredictability of chaotic output. This study found that under optical feedback conditions, NLs generate chaos across a wide range of feedback parameters, with the highly unpredictable region completely overlapping with the chaotic region. Further injection into the slave lasers enhances the chaotic output, expanding the range of unpredictability. Additionally, we analyzed the impact of internal parameter mismatch on the complexity of chaotic signals and found it to be similar to the scenario when parameters are matched. Using this chaotic system as an entropy source, we constructed a random number generator (RNG) and investigated the effects of internal parameters mismatch and differences in the injection parameters on the generator's performance. The simulation results show that the RNG performs well under different parameter settings, and the generated random sequences pass all random number tests successfully. Therefore, this chaotic system can yield a high-complexity chaotic light source with appropriate parameter selection, and when combined with effective post-processing, it can generate high-quality random numbers. This is crucial for advancing the realization of small-sized, high-randomness RNGs.

**Keywords:** nanolaser; random number generator; chaotic signal



**Citation:** Liu, G.; Mu, P.; Wang, K.; Guo, G.; Liu, X.; He, P. Random Numbers Generated Based on Dual-Channel Chaotic Light. *Electronics* **2024**, *13*, 1603. <https://doi.org/10.3390/electronics13091603>

Academic Editors: Christos Volos, Murilo da Silva Baptista, Lazaros Moysis and Marcin Lawnik

Received: 25 March 2024

Revised: 12 April 2024

Accepted: 16 April 2024

Published: 23 April 2024



**Copyright:** © 2024 by the authors. Licensee MDPI, Basel, Switzerland. This article is an open access article distributed under the terms and conditions of the Creative Commons Attribution (CC BY) license (<https://creativecommons.org/licenses/by/4.0/>).

## 1. Introduction

Random numbers have been widely applied in various fields of scientific research. In particular, random numbers play an irreplaceable role in diverse domains such as information verification [1,2], computer simulation [3], and secure communication [4–8]. According to the generation method, random numbers can be divided into two main categories: pseudo random numbers and physical random numbers. Pseudo random numbers [9,10] are generated based on deterministic algorithms and seeds, offering speed and convenience, with generation rates reaching Gb/s. However, these numbers are replicable and predictable, exhibiting drawbacks such as periodicity and repeatability. Consequently, systems relying on pseudo random number encryption are susceptible to attacks and security risks. Physical random numbers [11,12] are generated by using physical phenomena in nature as entropy sources, exhibiting a high degree of unpredictability. The main types of physical entropy sources include thermal noise [13,14], phase jitter in oscillating signals [15–17], chaos [18–21], and others. Amplifying signals based on thermal noise, selecting appropriate detection thresholds, and subsequent signal processing can ultimately generate true random numbers. Because thermal noise disturbances are small, high-gain amplifiers are required, but they are susceptible to external influences and lack stability. For the oscillator-based RNGs, random sources are the oscillator's phase jitter noise, which can achieve true random number output. However, it is not suitable for fully custom integrated circuits, and the randomness implemented in the circuit is relatively low.

In addition, the bandwidth of these physical entropy sources is limited, and the real-time generation rate of random numbers is only on the order of Mb/s. This limitation makes it challenging to meet the requirements of current high-speed, large-capacity communication and fast computational simulations.

Chaos has garnered widespread attention and research over the past few decades. Chaotic systems are renowned for their highly complex and unpredictable characteristics, which provide new insights and methods for random number generation. In recent years, there has been a significant amount of research on high-speed RNGs based on chaos [22–25]. Semiconductor lasers (SLs) are one of the most widely used light source devices, known for their advantages such as their simple structure, compact size, and reliable operation. Under external perturbations such as optical feedback [26], optical injection [27,28], or optoelectronic feedback [29,30], SLs can produce broadband chaotic laser outputs reaching several GHz. Scholars both domestically and internationally have conducted extensive research on using SLs for high-speed random number generation [31–34]. In 2008, Uchida et al., utilized laser chaos for the first time as a physical entropy source for random number extraction. After passing through a 1-bit analog-to-digital converter (ADC) and an exclusive-OR (XOR) operation, they achieved a RNG with a rate of 1.7 Gbit/s [35]. To increase the bit generation rate of random numbers, I. Reidler et al. employed an 8-bit ADC-based random number extraction scheme, resulting in the generation of a physical random number sequence with a rate of 12.5 Gbit/s [36]. In 2016, Butler et al. proposed an ultrafast RNG based on a semiconductor ring laser. By performing multi-bit sampling of chaotic optical waveforms and then applying a simple post-processing procedure, the generated random bit rate can reach 1 Tb/s [37]. In 2022, Guo et al. proposed an all-optical method for generating physical random bit sequences, achieving an online generated random bit stream with a speed of up to 10 Gbit/s [38]. The following year, Cai et al. utilized a distributed feedback laser to output two paths of complex optical chaotic signals. A dual-channel physical RNG with a bit rate on the order of terabits per second is implemented by combining a multi-bit extraction method [39].

However, the complex structure of traditional SLs and auxiliary materials makes it challenging to apply them to the practical photonics that integrated circuits need. With continuous innovation in science and technology, SLs have overcome these size limitations. The advent of nanolasers (NLs) has provided the possibility for photonics integration. When subjected to external disturbances, NLs exhibit dynamic characteristics that are similar to traditional SLs. Due to the extremely small mode volume of NLs, spontaneous emission is enhanced. Therefore, it is necessary to introduce characteristic factors into the rate equations to characterize spontaneous emission. Erwin first proposed introducing two important characteristic parameters, namely the Purcell factor  $F$  and the spontaneous emission coupling factor  $\beta$ , into traditional laser rate equations to characterize spontaneous emissions. Many studies have analyzed how these two characteristic factors affect the output properties of NLs. In 2012, Ding and Ning explored the effects of  $F$  and  $\beta$  on the performance of electronically pumped NLs [40]. Sattar et al. studied the nonlinear dynamical behavior of NLs under external optical feedback, phase-conjugate feedback, and optical injection [41–44]. In 2017, Han et al. analyzed the dynamic characteristics of mutually coupled NLs and investigated the influence of  $F$  and  $\beta$  on them [45,46]. The following year, Han et al. conducted a more in-depth analysis of the impact of high-frequency oscillations on mutually coupled NLs [47]. Elsonbaty et al. examined the time-delay signature (TDS) suppression in a single NL with a hybrid all-optical and electrooptic feedback scheme [48,49]. In 2019, Qu et al. investigated the impact of system parameters on TDS when dual-channel chaotic light is injected into NLs [50]. In the same year, Fan et al. conducted a numerical study on the stability of NLs with external optical feedback, exploring the influence of feedback phase on their stability [51]. In 2021, Li et al. separately analyzed the unpredictability of chaotic light sources under optical feedback and optical injection conditions. They investigated the impact of key parameters on the unpredictability of NL chaotic light sources [52]. The above studies extensively analyzed the dynamic char-

acteristics of NLs, providing inspiration for us to utilize nano-light sources for random number extraction. Due to the relatively short time since the emergence of NLs, there is currently limited research on the dynamic characteristics and related applications of NLs. Therefore, studying the chaotic dynamics of NLs contributes to a deeper understanding of the behavior and properties of nonlinear systems, expanding the application of chaos theory at the microscopic scale. As an important component of photonics, the chaotic dynamics of NLs are significant for integrating them into optical communication and random number generation devices, expanding the boundaries of their photonics applications, and enhancing the efficiency and security of optical information processing.

NLs have shown promising potential in the field of photonic integration, making them a hot topic of research. However, there have been relatively few reports on the applications of NLs. The main contribution of this paper is the proposal of a chaotic system based on NLs, which is successfully utilized as an entropy source for generating physical random numbers. This includes analyzing the chaotic region and unpredictability of the NLs under optical feedback and injection, particularly investigating the impact of parameter mismatch on NL characteristics. Building upon this, a RNG was constructed, successfully achieving high-speed physical random number generation, and the performance of the proposed RNG under different parameter settings was compared. The successful application of NLs in random number generation is crucial for realizing compact, high-quality RNGs.

The organization of this paper is as follows. In Section 2, we discuss the theoretical model of the RNG scheme. In Section 3, detailed numerical simulation results are presented. Firstly, we introduce two widely used measures, the 0–1 test for chaos and permutation entropy (PE), to analyze the influence of key parameters on the chaotic region and unpredictability of the the master laser (MNL) and the slave laser (SNL). This helps in determining the parameter range for obtaining highly unpredictable chaotic signals. Based on this analysis, a RNG was constructed, and the effects of parameters mismatch and injection parameter differences on the performance of random number generation were compared. In Section 4, conclusions are drawn. It is stated that the proposed chaotic system can output highly complex signals over a wide range of parameters. Therefore, by adjusting the appropriate parameters and employing effective post-processing techniques, high-quality random numbers can be generated. Furthermore, regarding parameter fluctuation, effective post-processing can successfully eliminate non-randomness in the generated random sequences.

## 2. Theoretical Model

The block diagram of the RNG is shown in Figure 1, where the chaotic entropy source of the RNG is composed of three NLs. The signal output from the MNL passes through the first polarization controller PC1 and arrives at the first fiber coupler FC1. At this point, a portion of the signal enters the feedback path, while another portion enters the injection path. The signal from the feedback loop is output from the first fiber coupler FC1, then it passes through the first variable optical attenuator VOA1 and fiber mirror FM before returning back to the MNL along the same path. By adjusting the feedback strength of the feedback path, the MNL can operate in a chaotic state, generating chaotic signals. The output from the injection path is split into the first injection path and the second injection path through the second fiber coupler FC2. Specifically, the signals from FC1 are output to an optical isolator OI, and after passing through it, the signals are divided into two parts by the second fiber coupler FC2. One part enters the first injection path, while the other part enters the second injection path. By controlling the injection strength of the signals in the first and second injection paths and adjusting the frequency detuning parameters of SNL1 and SNL2, enhanced chaotic signals are generated from SNL1 and SNL2, respectively. In the post-processing stage, the chaotic signals from the first and second injection paths are converted from optical signals to electrical signals by photodetectors. These signals are then subtracted from their delayed copies, and the resulting signals are converted into binary signals using 8-bit ADCs. The binary signals from both paths are combined through

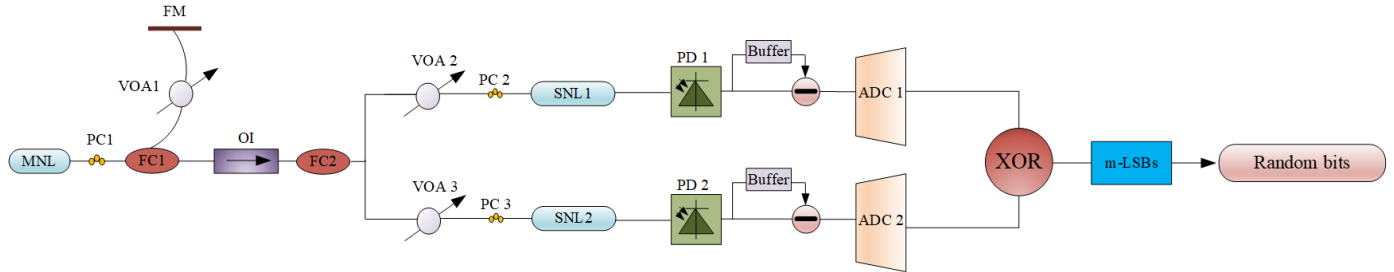


**Figure 1.** Block diagram of random number generation. PC1, PC2, and PC3: polarization controllers; FC1 and FC2: fiber couplers; FM, fiber mirror; VOA1, VOA2, and VOA3: variable optical attenuators; OI: optical isolator; PD1 and PD2: photodetectors; ADC1 and ADC2: analog-to-digital converters; m-LSBs: m least significant bits; XOR, exclusive-OR.

According to the device shown in Figure 1, the rate equations for the chaotic entropy source can be written as follows [41,43].

$$\frac{dI_M(t)}{dt} = \Gamma \left[ \frac{F\beta N_M(t)}{\tau_n} + \frac{g_n(N_M(t) - N_0)}{1 + \varepsilon I_M(t)} I_M(t) \right] - \frac{1}{\tau_p} I_M(t) + 2k_d \sqrt{I_M(t) I_M(t - \tau_d)} \cos(\theta_1(t)) \quad (1)$$

$$\frac{d\phi_M(t)}{dt} = \frac{\alpha}{2} \Gamma g_n(N_M(t) - N_{th}) - k_d \frac{\sqrt{I_M(t - \tau_d)}}{\sqrt{I_M(t)}} \sin(\theta_1(t)) \quad (2)$$

$$\frac{dN_M(t)}{dt} = \frac{I_{dc}}{eV_a} - \frac{N_M(t)}{\tau_n} (F\beta + 1 - \beta) - \frac{g_n(N_M(t) - N_0)}{1 + \varepsilon I_M(t)} I_M(t) \quad (3)$$

$$\begin{aligned} \frac{dI_{S1|S2}(t)}{dt} = & \Gamma \left[ \frac{F\beta N_{S1|S2}(t)}{\tau_n} + \frac{g_n(N_{S1|S2}(t) - N_0)}{1 + \varepsilon I_{S1|S2}(t)} I_{S1|S2}(t) \right] \\ & - \frac{1}{\tau_p} I_{S1|S2}(t) + 2k_{ri} \sqrt{I_{S1|S2}(t) I_{S1|S2}(t - \tau_{ri})} \cos(\theta_j(t)) \end{aligned} \quad (4)$$

$$\frac{d\phi_{S1|S2}(t)}{dt} = \frac{\alpha}{2} \Gamma g_n(N_{S1|S2}(t) - N_{th}) - 2\pi\Delta f_i - k_{ri} \frac{\sqrt{I_{S1|S2}(t - \tau_{ri})}}{\sqrt{I_{S1|S2}(t)}} \sin(\theta_j(t)) \quad (5)$$

$$\frac{dN_{S1|S2}(t)}{dt} = \frac{I_{dc}}{eV_a} - \frac{N_{S1|S2}(t)}{\tau_n} (F\beta + 1 - \beta) - \frac{g_n(N_{S1|S2}(t) - N_0)}{1 + \varepsilon I_{S1|S2}(t)} I_{S1|S2}(t) \quad (6)$$

$$\theta_1(t) = 2\pi f_M \tau_d + \phi_M(t) - \phi_M(t - \tau_d) \quad (7)$$

$$\theta_j(t) = 2\pi f_M \tau_{ri} + \phi_{S_i}(t) - \phi_M(t - \tau_{ri}) - 2\pi\Delta f_i t \quad (i = 1, 2; j = 2, 3) \quad (8)$$

In the above rate equations, the subscripts ‘M’, ‘S1’, and ‘S2’ represent the MNL, the first SNL, and the second SNL, respectively.  $I(t)$  is photon density,  $\phi(t)$  is the phase, and  $N(t)$  is carrier density. In this model, the key parameters are the Purcell factor  $F$  and the spontaneous emission coupling factor  $\beta$ . The NLs can exhibit enhanced dynamical performance, possibly arising from a combination of physical factors including  $F$  and  $\beta$ . The dc bias current is defined as  $I_{dc} = 2I_{th}$ , where  $I_{th}$  is the threshold current,  $e$  is the electron charge, and the threshold carrier density  $N_{th}$  ( $N_{th} = N_0 1/\Gamma g_n \tau_p$ ). The last term in Equations (1) and (2) represents the optical feedback and contains the feedback delay  $\tau_d$ . The feedback rate  $k_d$ .  $k_d$  can be written as follows [41]:

$$k_d = f(1 - R) \sqrt{\frac{R_{ext}}{R}} \frac{c}{2nL} \quad (9)$$

where  $f$  is the feedback coupling fraction,  $R$  stands for the reflectivity of the NLs,  $R_{ext}$  is the power reflectivity of the external mirror,  $c$  represents the speed of light in free space,  $n$  is the refractive index, and  $L$  denotes the cavity length of the NLs. The chaotic light source generated by optical feedback is further injected into the two SNLs. The last term in Equations (4) and (5) represents the optical injection, containing the injection rate  $k_{ri}$  and the injection delay  $\tau_{ri}$ .  $R_{inj}$  denotes the injection ratio, and  $k_{ri}$  can be written as follows [43]:

$$k_{ri} = (1 - R) \sqrt{\frac{R_{inj}}{R}} \frac{c}{2nL} \tag{10}$$

In addition, there is a frequency detuning  $\Delta f_i = f_M - f_{Si}$  between the MNL and SNL, where  $\Delta f_M$  and  $\Delta f_{Si}$  are the operating frequencies of the MNL and SNLs, respectively.

In this paper, for simplicity, the parameters set for the NLs are the same, meaning NLs with identical internal parameters, unless specifically stated to be different, such as in the subsequent discussion of parameter mismatch. Some of the key parameters used in the simulation are listed in Table 1 [41,43], and the remaining parameter values will be specified in the following sections.

**Table 1.** Parameters used in the simulations.

Parameters	Description	Value
$\lambda_0$	Wavelength of MNL	1591 nm
$L$	Cavity length	1.39 $\mu\text{m}$
$V_a$	Volume of active region	$3.96 \times 10^{-13} \text{ cm}^3$
$\Gamma$	Mode confinement factor	0.645
$Q$	Quality factor	428
$g_n$	Differential gain	$1.65 \times 10^{-6} \text{ cm}^3/\text{s}$
$\tau_p$	Photon lifetime	0.36 ps
$\tau_d$	Feedback delay	0.2 ns
$\tau_n$	Carrier lifetime	1 ns
$I_{th}$	Threshold current	1.127 mA
$N_0$	Transparency carrier density	$1.1 \times 10^{18} \text{ cm}^{-3}$
$\epsilon$	Gain saturation	$2.3 \times 10^{-17} \text{ cm}^3$
$n$	Refractive index	3.4
$\alpha$	Linewidth enhancement factor	5
$R_{ext}$	External factor power reflectivity	0.95
$R$	Laser facet reflectivity	0.85
$c$	Speed of light in free space	$3 \times 10^8 \text{ m/s}$
$F$	Cavity Purcell factor	14
$\beta$	Spontaneous emission coupling	0.05
$f$	Feedback coupling fraction	0.025

### 3. Results and Discussion

In this section, we utilize the fourth-order Runge–Kutta algorithm to integrate the rate equations and present the numerical simulation results.

#### 3.1. Effects of the Parameters on the Unpredictability of NLs

There are many methods available to distinguish between deterministic and chaotic dynamics [53]. Among these methods, the 0–1 chaos test [54] is a simple, fast, versatile, and effective method for assessing the chaotic properties of signals. It has excellent practicality and application potential and is of significant value and significance in fields such as chaos theory research, engineering applications, and information processing, where ‘0’ represents nonchaotic states and ‘1’ represents chaotic states. To quantify the corresponding complexity, this paper introduces the PE [55]. PE is a computational measure based on the coherence between adjacent data in a time series. Due to its simplicity and high robustness, it is widely used in the analysis of nonlinear systems and the calculation of sequence complexity. In chaotic systems, PE can serve as a measure of system complexity

and is applicable to any long time series, including chaotic signals, regular signals, and noise signals. The value of PE falls between 0 and 1. A higher value indicates a greater unpredictability, and consequently, the sequence is closer to a completely random sequence. Below, we will analyze the dynamical characteristics of the laser chaotic signal output from MNL and SNLs using 0–1 chaos testing and PE.

Since the output of MNL serves as the driving signal for the chaotic system, it is crucial to determine the chaotic region of MNL first. We utilize the 0–1 test for chaos and PE to investigate the dynamic characteristics of individual NLs under optical feedback. We analyze the influence of the feedback coupling fraction and feedback delay time on the chaotic region of the MNL. Figure 2 illustrates the changes in the chaotic region and complexity of the MNL under optical feedback when both the feedback delay time and feedback coupling fraction vary simultaneously. In Figure 2a, the chaotic region is represented in deep red, while the non-chaotic region is shown in blue. In Figure 2b, the highly unpredictable region is depicted in yellow, whereas the predictable region is in blue. It can be observed that the MNL under optical feedback generates chaos over a wide parameter space range. By observing the highly unpredictable region of the MNL, we find that the chaotic region completely overlaps with the highly unpredictable region. Therefore, by adjusting the feedback delay time and feedback coupling fraction, the dynamic output of the MNL can be easily controlled.

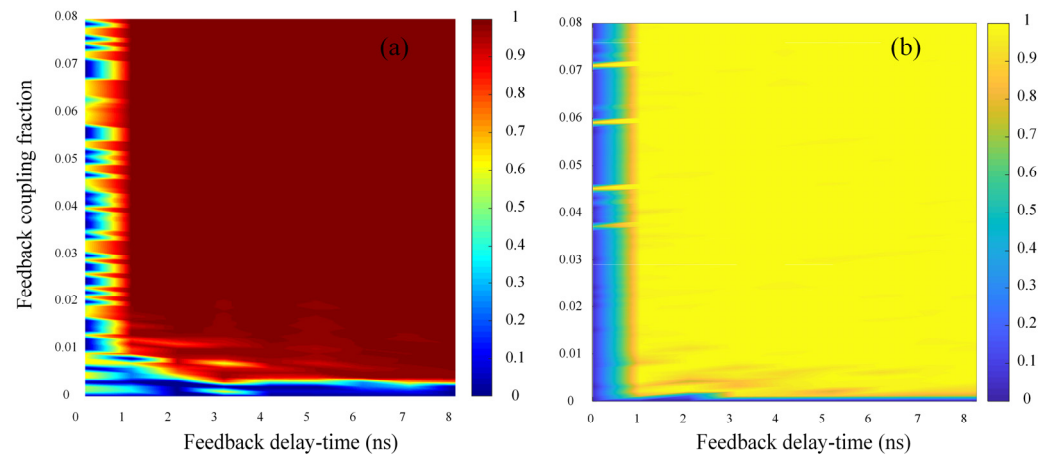


**Figure 2.** Two-dimensional map of the 0–1 test for chaos (a) and PE (b) of the MNL.

Building upon this, we also investigated the influence of the injection strength and frequency detuning on the chaotic regions of SNL1 and SNL2. In particular, we also considered the impact of parameter mismatch on the unpredictability of the chaotic light source. Here, the concept of the relative mismatch ratio is introduced, with the parameters of MNL and SNL1 set as fixed values, while the parameters of SNL2 vary with the relative mismatch ratio. The relative mis-match ratio is defined as follows [56]:

$$u = \frac{x_1 - x_2}{x_1} \tag{11}$$

In the above equation, the subscripts ‘1’ and ‘2’ denote the two slave lasers, respectively, and the variable  $x$  denotes the parameters, including the carrier lifetime  $\tau_n$ , differential gain  $g_n$ , photon lifetime  $\tau_p$ , linewidth enhancement factor  $\alpha$ , and transparency carrier density  $N_0$ . The equations for simultaneous mismatch of multiple parameters are as follows:

$$\tau_n^2 = (1 - u)\tau_n^1, g_n^2 = (1 - u)g_n^1, \tau_p^2 = (1 - u)\tau_p^1, \alpha^2 = (1 - u)\alpha^1, N_0^2 = (1 - u)N_0^1.$$

We set  $f = 0.025$  and  $\tau_d = 0.2$  ns to ensure that the output of the MNL is a highly complex chaotic signal, and then we unidirectionally inject it into SNL1 and SNL2. Since the output of the MNL is injected into two structurally identical NLs, we choose SNL1

to analyze its chaotic characteristics under matched parameters, with SNL2 serving as the control group for parameter mismatch. We set the relative mismatch rate as  $u = 0.05$ , analyzing the chaotic dynamical characteristics of SNL outputs under parameter matching and mismatching using 0–1 chaos testing and PE. Figure 3(a1,b1) depicts the results of the chaotic region when there are internal parameter matches and mismatches, respectively. It can be observed that the chaotic region is almost guaranteed across the entire parameter range. When the injection strength exceeds  $10 \text{ ns}^{-1}$ , the SNLs operate in a chaotic state, as the driving signal from the MNL is chaotic. Figure 3(a2,b2) describes the effects of the unpredictability changes on the injection strength and frequency detuning plane, with the highly complex region being entirely consistent with the chaotic region. Unpredictability is a crucial attribute of physical random numbers, which instills confidence in obtaining physical random numbers during subsequent random number extraction processes.

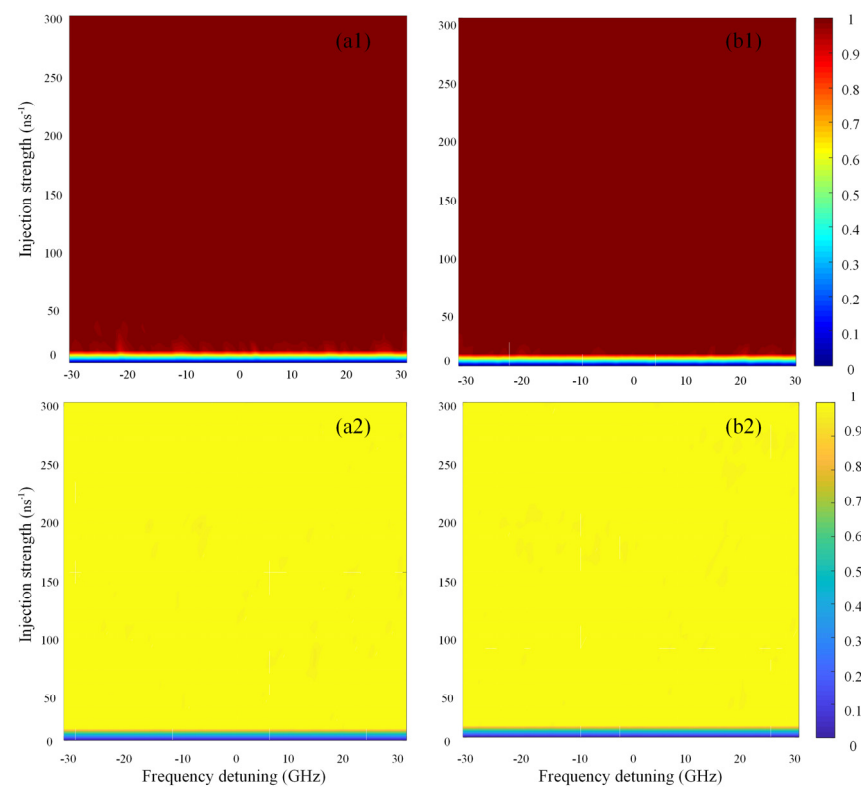


**Figure 3.** Two-dimensional map of the 0–1 test for chaos (a1,b1) and PE (a2,b2) for SNL1 (a) under internal parameter match conditions and for SNL2 (b) under internal parameter mismatch conditions.

### 3.2. Extracting Random Numbers

The stochastic characteristics of physical phenomena and post-processing jointly determine the unpredictability and statistical unbiasedness of random numbers. These consecutive sampling points are not independent, and there exists non-negligible correlations among them. Therefore, to extract high-quality random numbers from the chaotic entropy source, effective post-processing techniques must be employed. The purpose of post-processing is to enhance the randomness of the sequence and reduce the correlations between sequences. The statistical distribution characteristics of the entropy source initially will affect the randomness of the generated bit sequence. We use delay and differencing processing to make the entropy source after differencing conform to an ideal symmetric state. The XOR method is one of the simplest ways to address sequence correlation and uniformity, and it is widely employed in random number generation [31,33,35]. Specifically, this involves performing an XOR operation on a pair of bits from input data to produce a single output bit. Performing bitwise XOR operations on the two binary sequences can further eliminate bias and disrupt the remaining correlations. Extracting the LSBs is a com-

mon and simple yet effective post-processing method. It not only efficiently enhances the uniformity of the statistical distribution of the bit sequence but also disrupts any remaining correlations. The statistical characteristics of laser chaotic signals also play a role in determining the rate of the RNG. This is because the better the uniformity of the laser chaotic signal, the more bits of LSB can be utilized to generate the random number sequence. In the field of high-speed RNGs based on SL chaotic signals, numerous multi-bit post-processing schemes have been proposed. The central idea in these schemes is to transform the chaotic signal into a higher-resolution signal, followed by a series of post-processing steps to retain more LSBs, aiming to increase the random number generation rate.

The number of LSB bits extracted is based on the ability of the generated bit sequence to pass the random number test criterion. There are many methods and standards for random number sequence testing, mainly for the verification of the randomness of the generated random sequences. In this paper, the NIST SP 800-22 test standard is used [57]. NIST SP 800-22 is a random number test standard provided by the National Institute of Standards and Technology. The random code sequence testing program provided by NIST consists of a total of 15 tests. By sequentially testing the random sequence, the program assesses whether the sequence can pass all the test procedures to determine whether the RNG is a physical RNG. As advised by the NIST SP 800-22, we perform each test with 1000 samples of 1 Mbit binary numbers with a significance level of  $\alpha = 0.01$ . For a 1 Mbit sample, each test yields a  $p$ -value. Based on 1000  $p$ -values, the pass rate and the uniformity level of the  $p$ -value distribution can be calculated, denoted as proportion and  $p$ -value, respectively. A random bit sequence is said to pass the NIST test if the  $p$ -value for each test is larger than 0.0001 and the proportion of samples passing each test is within the range of  $0.99 \pm 0.0094392$ .

The number of LSBs retained depends on whether the generated bit sequence can pass the NIST random number test. The good statistical properties of chaotic entropy sources and effective post-processing can ensure that more LSBs are used to generate random number sequences. By studying the relationship between the number of retained LSBs and the results of random number tests, the influence of relevant parameters on RNG performance can be investigated.

### 3.2.1. Internal Parameter Matching

Firstly, without considering the internal parameter mismatch (i.e., all NLs have the same internal parameters), we studied the impact of identical and different injection parameters on RNG performance. As the statistical properties of chaotic laser signals can affect the performance of random number extraction, we adjust the frequency detuning and injection strength to make the statistical properties of the chaotic signal as close as possible to a symmetric distribution. When the injection parameters are identical, the relevant parameter settings are as follows:  $\Delta f_1 = \Delta f_2 = -5$  GHz,  $k_{r1} = k_{r2} = 210$  ns<sup>-1</sup>. When the injection parameters are different, the relevant parameter settings are as follows:  $\Delta f_1 = -5$  GHz,  $\Delta f_2 = -10$  GHz,  $k_{r1} = 210$  ns<sup>-1</sup>,  $k_{r2} = 220$  ns<sup>-1</sup>. Under the given simulation parameters and without considering gain saturation effects, the amplitude distribution of the chaotic entropy source exhibits asymmetry. We differentiate the original chaotic signal from itself after a certain delay time to obtain the delayed differential chaotic entropy source. As shown in Figure 4, the statistical distribution histogram of the differentially processed entropy source conforms to a symmetric distribution.

When the internal parameters of the NLs are matched, we set the injection parameters to be the same. SNL1 and SNL2 will produce identical chaotic time series. Therefore, further post-processing is required. The signal after delayed differentiation is quantized into an 8-bit binary sequence through an 8-bit ADC (ADC sampling rate of 80 GHz). Performing bit shifting on the binary sequence in the SNL2 channel. A bitwise XOR operation is performed between the binary sequence in SNL1 pathway and the binary sequence after shifting in SNL2 pathway to obtain an 8-bit binary sequence. Figure 5 shows the histogram of statistical distributions when retaining different numbers of LSBs under

identical injection parameters. Under different injection parameters, the output of the chaotic signal is completely different, thus eliminating the need for shifting processing. Figure 6 shows the histogram of statistical distributions when retaining different numbers of LSBs under different injection parameters. Observing Figures 5 and 6 reveals the same trend: even when discarding the most significant bit, the amplitude distribution remains extremely asymmetric. As the number of retained least significant bits decreases, the uniformity of the amplitude distribution gradually improves.

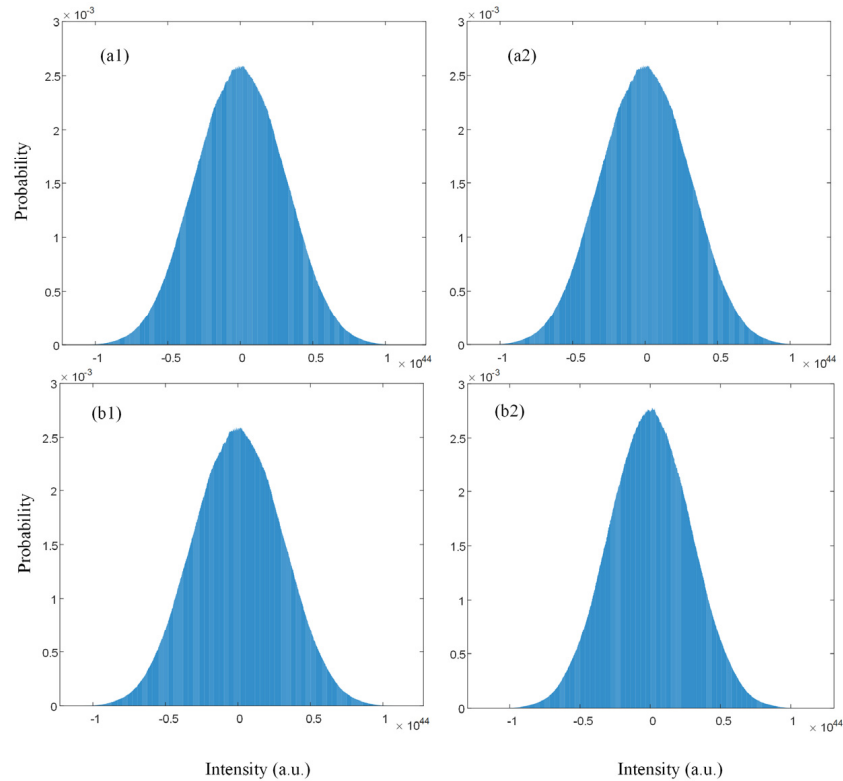


**Figure 4.** Amplitude distribution of chaotic signals after delayed differencing of SNLs under identical injection parameters (a) and different injection parameters (b), where SNL1 (a1,b1) and SNL2 (a2,b2).

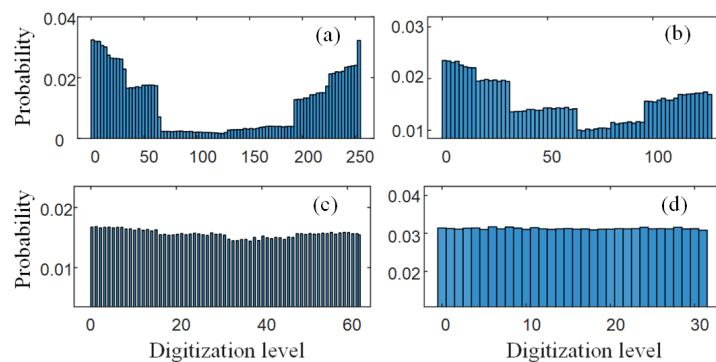


**Figure 5.** Statistical histogram of the retained m-LSBs under identical injection parameters: (a) m = 8; (b) m = 7; (c) m = 6; (d) m = 5.

Due to the highly uneven statistical distribution when retaining 8-LSBs and 7-LSBs, we opted to begin random number testing by retaining 6-LSBs. Under identical injection parameters, the random bit sequence obtained using the retained 6-LSBs only passed 6 tests. By discarding one LSB, i.e., retaining 5-LSBs, the resulting random sequence passed 13 tests. When retaining 4-LSBs, it passed all the tests. Under different injection parameters, the random number sequence generated using the retained 6-LSBs passed

12 tests. We discarded one LSB, i.e., retained 5-LSBs, and continued testing. The random number sequence generated using the retained 5-LSBs passed all the tests. The successful test results are presented in Table 2. When the injection parameters are different, an extra LSB can be retained. This is because when the injection parameters are the same, there is still a strong correlation between the shifted sequence in the SNL2 path and the unshifted sequence in the SNL1 path.

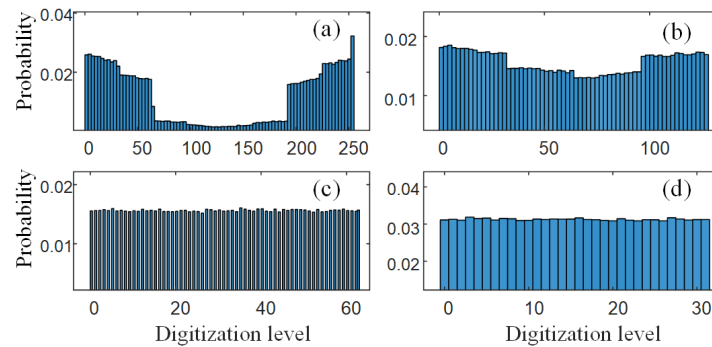


**Figure 6.** Statistical histogram of the retained *m*-LSBs under different injection parameters: (a) *m* = 8; (b) *m* = 7; (c) *m* = 6; (d) *m* = 5.

**Table 2.** Results of NIST statistical tests under matched internal parameters.

Statistical Test	Retaining 4-LSBs under Identical Injection Parameters			Retaining 5-LSBs under Different Injection Parameters		
	<i>p</i> -Value	Proportion	Result	<i>p</i> -Value	Proportion	Result
Frequency	0.344048	0.989	Success	0.344048	0.989	Success
Block frequency	0.136399	0.993	Success	0.136399	0.993	Success
Cumulative sums	0.739918	0.990	Success	0.739918	0.990	Success
Runs	0.779188	0.986	Success	0.779188	0.986	Success
Longest runs	0.599693	0.989	Success	0.599693	0.989	Success
Rank	0.320607	0.991	Success	0.320607	0.991	Success
Fast Fourier transform	0.461612	0.990	Success	0.461612	0.990	Success
Non-overlapping template	0.192724	0.981	Success	0.192724	0.981	Success
Overlapping template	0.236810	0.997	Success	0.236810	0.997	Success
Universal	0.117432	0.987	Success	0.117432	0.987	Success
Approximate entropy	0.476911	0.986	Success	0.476911	0.986	Success
Random excursions	0.057593	0.987	Success	0.057593	0.987	Success
Random excursions variant	0.063864	0.987	Success	0.063864	0.987	Success
Serial	0.258307	0.990	Success	0.258307	0.990	Success
Linear complexity	0.836048	0.994	Success	0.836048	0.994	Success

### 3.2.2. Internal Parameter Mismatch

In this section, we investigate the performance of the RNG under parameter mismatch when the injection parameters are identical and different. The parameters of the MNL and SNL1 are set as fixed values, while the parameters of SNL2 vary with the relative mismatch ratio, where  $u = 0.05$ . The parameters for the identical injection parameters are set as follows:  $\Delta f_1 = \Delta f_2 = -5$  GHz,  $k_{r1} = k_{r2} = 160$  ns<sup>-1</sup>. The parameters for the different injection parameters are set as follows:  $\Delta f_1 = -5$  GHz,  $\Delta f_2 = -10$  GHz,  $k_{r1} = 160$  ns<sup>-1</sup>,  $k_{r1} = 170$  ns<sup>-1</sup>. The amplitude distribution of the original chaotic signals still exhibits asymmetry. We applied delayed differentiation processing, and the amplitude distributions of the chaotic entropy source after delayed differentiation are shown in Figure 7, which conforms to a symmetric distribution.

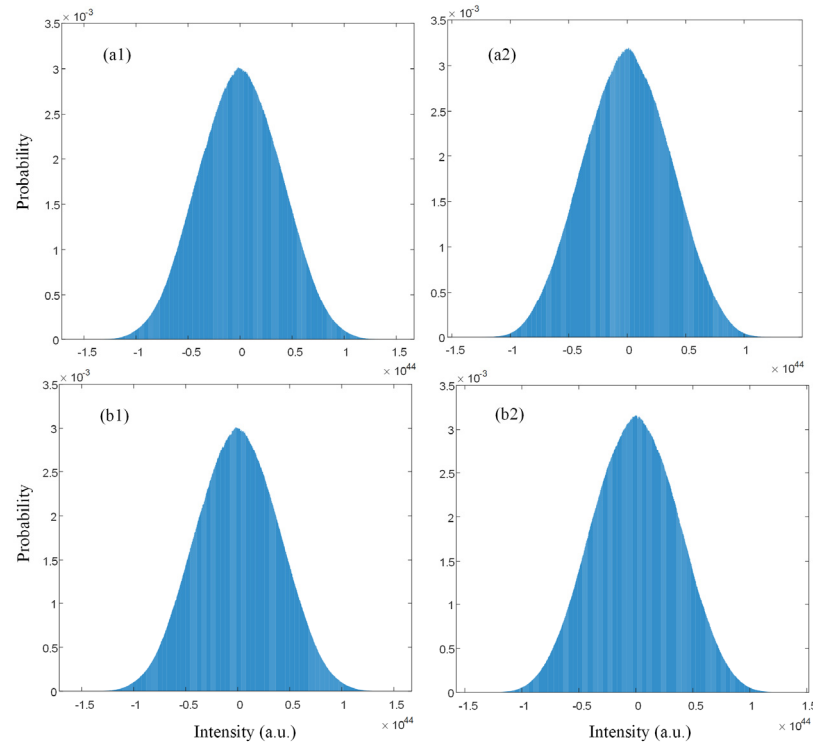


**Figure 7.** Amplitude distribution of chaotic signals after delayed differencing of SNLs under identical injection parameters (a) and different injection parameters (b), where SNL1 (a1,b1) and SNL2 (a2,b2).

The delayed differentiated signal was sampled and quantized using an 8-bit ADC (ADC sampling rate of 100 GHz), converting it into 8-bit binary code. Through XOR operation and retaining the LSB, we ultimately obtained the random bit sequence. Figures 8 and 9 display the histograms of the statistical distribution of the LSB extraction when the injection parameters are identical and different under parameter mismatch, respectively. It can be observed that as the number of retained LSBs decreases, the amplitude distribution tends to balance. Therefore, we still chose to start testing from the retained 6-LSBs.

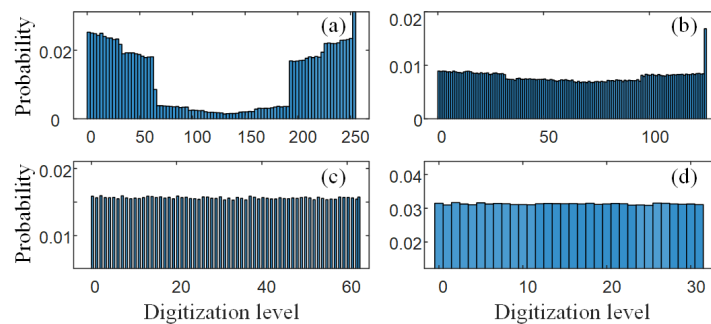


**Figure 8.** Statistical histogram of the retained m-LSBs under identical injection parameters: (a) m = 8; (b) m = 7; (c) m = 6; (d) m = 5.

When the injection parameters were identical, retaining 6-LSBs resulted in only one failed test. By discarding one LSB, i.e., retaining 5-LSBs, the generated sequence passed all the tests. When the injection parameters were different, retaining 6-LSBs resulted in two failed tests. Retaining 5-LSBs enabled the generated sequence to pass all the tests. The successful test results are shown in Table 3.

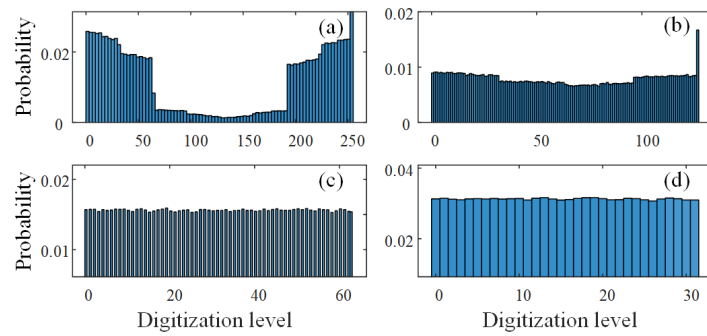


**Figure 9.** Statistical histogram of the retained m-LSBs under different injection parameters: (a)  $m = 8$ ; (b)  $m = 7$ ; (c)  $m = 6$ ; (d)  $m = 5$ .

**Table 3.** Results of NIST statistical tests under mismatched internal parameters.

Statistical Test	Retaining 5-LSBs under Identical Injection Parameters			Retaining 5-LSBs under Different Injection Parameters		
	<i>p</i> -Value	Proportion	Result	<i>p</i> -Value	Proportion	Result
Frequency	0.723804	0.984	Success	0.125927	0.987	Success
Block frequency	0.811080	0.990	Success	0.385543	0.995	Success
Cumulative sums	0.185555	0.985	Success	0.010531	0.987	Success
Runs	0.620465	0.989	Success	0.008090	0.990	Success
Longest runs	0.033362	0.990	Success	0.546283	0.989	Success
Rank	0.212184	0.993	Success	0.668321	0.992	Success
Fast Fourier transform	0.998655	0.986	Success	0.798139	0.991	Success
Non-overlapping template	0.009880	0.993	Success	0.620465	0.983	Success
Overlapping template	0.016037	0.987	Success	0.034712	0.987	Success
Universal	0.560545	0.982	Success	0.054661	0.987	Success
Approximate entropy	0.355364	0.986	Success	0.812905	0.982	Success
Random excursions	0.280306	0.983	Success	0.213309	0.989	Success
Random excursion variants	0.321625	0.985	Success	0.422521	0.987	Success
Serial	0.482707	0.987	Success	0.123755	0.985	Success
Linear complexity	0.801865	0.994	Success	0.731886	0.988	Success

Based on the simulation results above, retaining 5-LSBs under mismatched parameters, both with identical and different injection parameters, allowed the generated sequence to pass the random number tests. Compared to the RNG test results under parameter matching, the RNG still performs well under parameter mismatch conditions. Therefore, even in the presence of parameter fluctuations, non-randomness in the random sequence can be eliminated through post-processing in the proposed scheme. Comparing physical RNGs based on thermal noise [13,14] and phase jitter [15–17], although they can generate high-quality random numbers, their outputs are unstable, and the generation rates are relatively low. The RNG proposed in this paper based on laser chaos has significantly improved generation rates and exhibits good stability. Additionally, NLs have the advantages of a small size, easy integration, and modulation capabilities, demonstrating excellent nonlinear dynamic characteristics. This study provides valuable experience for high-speed random number generation in the field of photonic integration.

#### 4. Conclusions

This paper proposed a chaotic system based on novel NLs. Through 0–1 testing for chaos and PE, a systematic analysis of the chaotic region of the NLs was conducted, exploring in detail the influence of key parameters on the unpredictability of the output from the NLs. This research revealed that under optical feedback conditions, the MNL generates chaos over a wide range of parameters, and the high unpredictability region completely overlaps with the chaotic region. Further optical injection enhances the chaotic output, expanding the range of unpredictability. Additionally, we analyzed the influence of internal parameter mismatch on the complexity of the chaotic signal and found that its chaotic characteristics remained similar to when the parameters were matched. Using a chaotic light source with a high complexity and symmetric amplitude distribution as an entropy source, we constructed a RNG. We investigated the impact of internal parameters mismatch and external injection parameter differences on the performance of the RNG. The simulation results showed that the RNG performed well under different parameter settings, and the generated random sequences passed all the random number tests successfully. Regarding the parameter fluctuations of the NLs, the proposed post-processing steps effectively eliminated non-randomness in the random sequence. Compared to RNGs based on traditional physical entropy sources, RNGs based on NLs offer advantages such as a smaller size, ease of control, and faster generation rates. They provide valuable insights and references for obtaining high-speed random numbers using NLs in the field of photonic integration. NLs have potential applications in photonic integrated circuits, optical information processing, and system-on-chip technologies. The dynamic output generated by NLs, especially the optimization and application of chaotic light sources produced by NLs, will also become a hot research topic. In the future, there will be in-depth exploration of the nonlinear dynamical characteristics of NLs, with additional experiments aimed at validating the superiority of NL-generated chaotic light sources. Additionally, there will be further exploration applications of NLs in random number generation.

**Author Contributions:** Methodology, G.L. and P.M.; validation, P.M., G.G. and X.L.; investigation, G.L., K.W. and P.H.; writing—original draft preparation, G.L., G.G., X.L. and K.W.; writing—review and editing, G.L., P.M., K.W. and P.H. All authors have read and agreed to the published version of the manuscript.

**Funding:** This research was funded by the Project: Natural Science Foundation of Shandong Provincial (ZR2020QF090), The Key Lab of Modern Optical Technologies of Education Ministry of China, Soochow University (KJS2066); The Key Lab of Advanced Optical Manufacturing Technologies of Jiangsu Province, Soochow University (KJS2045).

**Data Availability Statement:** Data are contained within the article.

**Conflicts of Interest:** Author Gang Guo and Xintian Liu were employed by the company FISEC Infomation Technology Company Limited. The remaining authors declare that the research was conducted in the absence of any commercial or financial relationships that could be construed as a potential conflict of interest.

#### References

1. Liu, B.; Yang, B.; Su, X. An Improved Two-Way Security Authentication Protocol for RFID System. *Information* **2018**, *9*, 86. [[CrossRef](#)]
2. Yu, F.; Li, L.; Tang, Q.; Cai, S.; Song, Y.; Xu, Q. A Survey on True Random Number Generators Based on Chaos. *Discrete Dyn. Nat. Soc.* **2019**, *2019*, e2545123. [[CrossRef](#)]
3. Dang, B.; Sun, J.; Zhang, T.; Wang, S.; Zhao, M.; Liu, K.; Xu, L.; Zhu, J.; Cheng, C.; Bao, L.; et al. Physically Transient True Random Number Generators Based on Paired Threshold Switches Enabling Monte Carlo Method Applications. *IEEE Electron Device Lett.* **2019**, *40*, 1096–1099. [[CrossRef](#)]
4. Cheng, G.; Wang, C.; Chen, H. A Novel Color Image Encryption Algorithm Based on Hyperchaotic System and Permutation-Diffusion Architecture. *Int. J. Bifurc. Chaos* **2019**, *29*, 1950115. [[CrossRef](#)]
5. Zhou, L.; Tan, F.; Yu, F. A Robust Synchronization-Based Chaotic Secure Communication Scheme with Double-Layered and Multiple Hybrid Networks. *IEEE Syst. J.* **2020**, *14*, 2508–2519. [[CrossRef](#)]

6. Gu, K.; Jia, W.; Wang, G.; Wen, S. Efficient and Secure Attribute-Based Signature for Monotone Predicates. *Acta Inform.* **2017**, *54*, 521–541. [[CrossRef](#)]
7. Xia, Z.; Fang, Z.; Zou, F.; Wang, J.; Sangaiah, A.K. Research on Defensive Strategy of Real-Time Price Attack Based on Multiperson ZeroDeterminant. *Secur. Commun. Netw.* **2019**, *2019*, e6956072. [[CrossRef](#)]
8. Gu, K.; Wu, N.; Yin, B.; Jia, W. Secure Data Query Framework for Cloud and Fog Computing. *IEEE Trans. Netw. Serv. Manag.* **2020**, *17*, 332–345. [[CrossRef](#)]
9. Yu, F.; Li, L.; He, B.; Liu, L.; Qian, S.; Huang, Y.; Cai, S.; Song, Y.; Tang, Q.; Wan, Q.; et al. Design and FPGA Implementation of a Pseudorandom Number Generator Based on a Four-Wing Memristive Hyperchaotic System and Bernoulli Map. *IEEE Access* **2019**, *7*, 181884–181898. [[CrossRef](#)]
10. Rezk, A.A.; Madian, A.H.; Radwan, A.G.; Soliman, A.M. Reconfigurable Chaotic Pseudo Random Number Generator Based on FPGA. *AEU—Int. J. Electron. Commun.* **2019**, *98*, 174–180. [[CrossRef](#)]
11. Abutaleb, M.M. A Novel True Random Number Generator Based on QCA Nanocomputing. *Nano Commun. Netw.* **2018**, *17*, 14–20. [[CrossRef](#)]
12. Hasan, R.S.; Tawfeeq, S.K.; Mohammed, N.Q.; Khaleel, A.I. A True Random Number Generator Based on the Photon Arrival Time Registered in a Coincidence Window between Two Single-Photon Counting Modules. *Chin. J. Phys.* **2018**, *56*, 385–391. [[CrossRef](#)]
13. Kim, E.; Lee, M.; Kim, J.-J. 8.2 Mb/s 28Mb/mJ Robust True-Random-Number Generator in 65nm CMOS Based on Differential Ring Oscillator with Feedback Resistors. In Proceedings of the 2017 IEEE International SolidState Circuits Conference (ISSCC), San Francisco, CA, USA, 5–9 February 2017; pp. 144–145.
14. Drutarovsky, M.; Galajda, P. A Robust Chaos-Based True Random Number Generator Embedded in Reconfigurable Switched-Capacitor Hardware. In Proceedings of the 2007 17th International Conference Radioelektronika, Brno, Czech Republic, 24–25 April 2007; pp. 1–6.
15. Yang, Y.; Bai, G.; Chen, H. A 200Mbps Random Number Generator with Jitter-Amplified Oscillator. In Proceedings of the Fifth International Conference on Computing, Communications and Networking Technologies (ICCCNT), Hefei, China, 11–13 July 2014; pp. 1–5.
16. Bejar, E.; Saldaña, J.; Raygada, E.; Silva, C. On the Jitter-to-Fast-Clock-Period Ratio in Oscillator-Based True Random Number Generators. In Proceedings of the 2017 24th IEEE International Conference on Electronics, Circuits and Systems (ICECS), Batumi, Georgia, 5–8 December 2017; pp. 243–246.
17. Amaki, T.; Hashimoto, M.; Onoye, T. Jitter Amplifier for Oscillator-Based True Random Number Generator. *IEICE Trans. Fundam. Electron. Commun. Comput. Sci.* **2013**, *E96-A*, 684–696. [[CrossRef](#)]
18. Yu, F.; Gao, L.; Gu, K.; Yin, B.; Wan, Q.; Zhou, Z. A Fully Qualified Four-Wing Four-Dimensional Autonomous Chaotic System and Its Synchronization. *Optik* **2017**, *131*, 79–88. [[CrossRef](#)]
19. Jin, J.; Zhao, L. Low Voltage Low Power Fully Integrated Chaos Generator. *J. Circuits Syst. Comput.* **2018**, *27*, 1850155. [[CrossRef](#)]
20. Zhou, L.; Wang, C.; Zhou, L. A Novel No-Equilibrium Hyperchaotic Multi-Wing System via Introducing Memristor. *Int. J. Circuit Theory Appl.* **2018**, *46*, 84–98. [[CrossRef](#)]
21. Zhou, L.; Wang, C.; Zhang, X.; Yao, W. Various Attractors, Coexisting Attractors and Antimonotonicity in a Simple Fourth-Order Memristive Twin-T Oscillator. *Int. J. Bifurc. Chaos* **2018**, *28*, 1850050. [[CrossRef](#)]
22. Park, M.; Rodgers, J.C.; Lathrop, D.P. True Random Number Generation Using CMOS Boolean Chaotic Oscillator. *Microelectron. J.* **2015**, *46*, 1364–1370. [[CrossRef](#)]
23. Çiçek, İ.; Dündar, G. A Chaos Based Integrated Jitter Booster Circuit for True Random Number Generators. In Proceedings of the 2013 European Conference on Circuit Theory and Design (ECCTD), Dresden, Germany, 8–12 September 2013; pp. 1–4.
24. Mu, P.; Pan, W.; Xiang, S.; Li, N.; Liu, X.; Zou, X. Fast Physical and Pseudo Random Number Generation Based on a Nonlinear Optoelectronic Oscillator. *Mod. Phys. Lett. B* **2015**, *29*, 1550142. [[CrossRef](#)]
25. Akgul, A.; Caglan, H.; Koyuncu, I.; Pehlivan, I.; Istanbulu, A. Chaos-Based Engineering Applications with a 3D Chaotic System without Equilibrium Points. *Nonlinear Dyn.* **2016**, *84*, 481–495. [[CrossRef](#)]
26. Liu, B.; Jiang, Y.; Ji, H. Sensing by Dynamics of Lasers with External Optical Feedback: A Review. *Photonics* **2022**, *9*, 450. [[CrossRef](#)]
27. Komarov, A.; Komarov, K.; Niang, A.; Sanchez, F. Nature of Soliton Interaction in Fiber Lasers with Continuous External Optical Injection. *Phys. Rev. A* **2014**, *89*, 013833. [[CrossRef](#)]
28. Yaronova, E.A.; Krents, A.A.; Molevich, N.E.; Anchikov, D.A. Suppression of Spatiotemporal Instabilities in BroadArea Lasers with Pump Modulation by External Optical Injection. *Bull. Lebedev Phys. Inst.* **2021**, *48*, 55–58. [[CrossRef](#)]
29. Tang, S.; Liu, J.M. Chaotic Pulsing and Quasi-Periodic Route to Chaos in a Semiconductor Laser with Delayed Opto-Electronic Feedback. *IEEE J. Quantum Electron.* **2001**, *37*, 329–336. [[CrossRef](#)]
30. Saboureau, P.; Foing, J.-P.; Schanne, P. Injection-Locked Semiconductor Lasers with Delayed Optoelectronic Feedback. *IEEE J. Quantum Electron.* **1997**, *33*, 1582–1591. [[CrossRef](#)]
31. Tang, X.; Wu, J.; Xia, G.; Wu, Z. 17.5 Gbit/s Random Bit Generation Using Chaotic Output Signal of Mutually Coupled Semiconductor Lasers. *Acta Phys. Sin.* **2011**, *60*, 110509. [[CrossRef](#)]
32. Kanter, I.; Aviad, Y.; Reidler, I.; Cohen, E.; Rosenbluh, M. An Optical Ultrafast Random Bit Generator. *Nat. Photonics* **2010**, *4*, 58–61. [[CrossRef](#)]
33. Tang, X.; Wu, Z.M.; Wu, J.G.; Deng, T.; Chen, J.J.; Fan, L.; Zhong, Z.Q.; Xia, G.Q. Tbits/s Physical Random Bit Generation Based on Mutually Coupled Semiconductor Laser Chaotic Entropy Source. *Opt. Express* **2015**, *23*, 33130–33141. [[CrossRef](#)] [[PubMed](#)]

34. Li, N.; Kim, B.; Chizhevsky, V.N.; Locquet, A.; Bloch, M.; Citrin, D.S.; Pan, W. Two Approaches for Ultrafast Random Bit Generation Based on the Chaotic Dynamics of a Semiconductor Laser. *Opt. Express* **2014**, *22*, 6634–6646. [[CrossRef](#)]
35. Uchida, A.; Amano, K.; Inoue, M.; Hirano, K.; Naito, S.; Someya, H.; Oowada, I.; Kurashige, T.; Shiki, M.; Yoshimori, S.; et al. Fast Physical Random Bit Generation with Chaotic Semiconductor Lasers. *Nat. Photonics* **2008**, *2*, 728–732. [[CrossRef](#)]
36. Reidler, I.; Aviad, Y.; Rosenbluh, M.; Kanter, I. Ultrahigh-Speed Random Number Generation Based on a Chaotic Semiconductor Laser. *Phys. Rev. Lett.* **2009**, *103*, 024102. [[CrossRef](#)] [[PubMed](#)]
37. Butler, T.; Durkan, C.; Goulding, D.; Slepneva, S.; Kelleher, B.; Hegarty, S.P.; Huyet, G. Optical Ultrafast Random Number Generation at 1 Tb/s Using a Turbulent Semiconductor Ring Cavity Laser. *Opt. Lett.* **2016**, *41*, 388–391. [[CrossRef](#)] [[PubMed](#)]
38. Guo, Y.; Cai, Q.; Li, P.; Zhang, R.; Xu, B.; Shore, K.A.; Wang, Y. Ultrafast and Real-Time Physical Random Bit Extraction with All-Optical Quantization. *Adv. Photonics* **2022**, *4*, 035001. [[CrossRef](#)]
39. Cai, Q.; Li, P.; Shi, Y.; Jia, Z.; Ma, L.; Xu, B.; Chen, X.; Alan Shore, K.; Wang, Y. Tbps Parallel Random Number Generation Based on a Single Quarter-Wavelength-Shifted DFB Laser. *Opt. Laser Technol.* **2023**, *162*, 109273. [[CrossRef](#)]
40. Ding, K.; Ning, C.Z. Metallic Subwavelength-Cavity Semiconductor Nanolasers. *Light Sci. Appl.* **2012**, *1*, e20. [[CrossRef](#)]
41. Abdul Sattar, Z.; Shore, K.A. External Optical Feedback Effects in Semiconductor Nanolasers. *IEEE J. Sel. Top. Quantum Electron.* **2015**, *21*, 500–505. [[CrossRef](#)]
42. Sattar, Z.A.; Shore, K.A. Dynamics of Nanolasers Subject to Optical Injection and Optical Feedback. In *Proceedings of the Physics and Simulation of Optoelectronic Devices XXIV*; SPIE: Bellingham, WA, USA, 2016; Volume 9742, pp. 38–47.
43. Abdul Sattar, Z.; Ali Kamel, N.; Shore, K.A. Optical Injection Effects in Nanolasers. *IEEE J. Quantum Electron.* **2016**, *52*, 1200108. [[CrossRef](#)]
44. Abdul Sattar, Z.; Shore, K.A. Phase Conjugate Feedback Effects in Nano-Lasers. *IEEE J. Quantum Electron.* **2016**, *52*, 1100108. [[CrossRef](#)]
45. Han, H.; Shore, K.A. Dynamical Characteristics of Nano-Lasers Subject to Optical Injection and Phase Conjugate Feedback. *IET Optoelectron.* **2018**, *12*, 25–29. [[CrossRef](#)]
46. Han, H.; Shore, K.A. Modulated Mutually Coupled NanoLasers. *IEEE J. Quantum Electron.* **2017**, *53*, 1–8. [[CrossRef](#)]
47. Han, H.; Shore, K.A. Analysis of High-Frequency Oscillations in Mutually-Coupled NanoLasers. *Opt. Express* **2018**, *26*, 10013–10022. [[CrossRef](#)] [[PubMed](#)]
48. Elsonbaty, A.; Hegazy, S.F.; Obayya, S.S. Simultaneous Concealment of Time Delay Signature in Chaotic Nanolaser with Hybrid Feedback. *Opt. Lasers Eng.* **2018**, *107*, 342–351. [[CrossRef](#)]
49. Elsonbaty, A.; Hegazy, S.F.; Obayya, S.S.A. Time Delay Signature of Chaotic Nanolasers and Its Concealment. In *Proceedings of the 2017 International Applied Computational Electromagnetics Society Symposium—Italy (ACES)*, Firenze, Italy, 26–30 March 2017; pp. 1–2.
50. Qu, Y.; Xiang, S.; Wang, Y.; Lin, L.; Wen, A.J.; Hao, Y. Concealment of Time Delay Signature of Chaotic Semiconductor Nanolasers with Double Chaotic Optical Injections. *IEEE J. Quantum Electron.* **2019**, *55*, 1–7. [[CrossRef](#)]
51. Fan, Y.; Hong, Y.; Li, P. Numerical Investigation on Feedback Insensitivity in Semiconductor Nanolasers. *IEEE J. Sel. Top. Quantum Electron.* **2019**, *25*, 1–7. [[CrossRef](#)]
52. Jiang, P.; Zhou, P.; Li, N.; Mu, P.; Li, X. Time Delay Concealment and Unpredictability Enhancement of Nanolasers under External Cavity Regulation. *ACTA Phys. Sin.* **2021**, *70*, 11. [[CrossRef](#)]
53. Li, N.; Susanto, H.; Cemlyn, B.R.; Henning, I.D.; Adams, M.J. Stability and Bifurcation Analysis of Spin-Polarized Vertical-Cavity Surface-Emitting Lasers. *Phys. Rev. A* **2017**, *96*, 013840. [[CrossRef](#)]
54. Gottwald, G.A.; Melbourne, I. On the Implementation of the 0–1 Test for Chaos. *SIAM J. Appl. Dyn. Syst.* **2009**, *8*, 129–145. [[CrossRef](#)]
55. Bandt, C.; Pompe, B. Permutation Entropy: A Natural Complexity Measure for Time Series. *Phys. Rev. Lett.* **2002**, *88*, 174102. [[CrossRef](#)]
56. Li, N.; Pan, W.; Yan, L.; Luo, B.; Xu, M.; Tang, Y.; Jiang, N.; Xiang, S.; Zhang, Q. Chaotic Optical Cryptographic Communication Using a Three-Semiconductor-Laser Scheme. *JOSA B* **2012**, *29*, 101–108. [[CrossRef](#)]
57. *Special Publication (NIST SP) 800-22 Rev 1a*; A Statistical Test Suite for Random and Pseudorandom Number Generators for Cryptographic Applications. National Institute of Standards and Technology: Gaithersburg, MD, USA, 2010.

**Disclaimer/Publisher’s Note:** The statements, opinions and data contained in all publications are solely those of the individual author(s) and contributor(s) and not of MDPI and/or the editor(s). MDPI and/or the editor(s) disclaim responsibility for any injury to people or property resulting from any ideas, methods, instructions or products referred to in the content.